applied optics

# Nitrogen thermometry in an inductively coupled plasma torch using broadband nanosecond coherent anti-Stokes Raman scattering

Dan Fries,[1] Spenser T. Stark,[1] John S. Murray,[1] Rajkumar Bhakta,[2] Elijah R. Jans,[2] Noel T. Clemens,[1] Philip L. Varghese,[1] and Sean P. Kearney[2,*]

[1]Department of Aerospace Engineering and Engineering Mechanics, The University of Texas at Austin, Austin, Texas 78712, USA
[2]Engineering Sciences Center, Sandia National Laboratories, Albuquerque, New Mexico 87123, USA
*spkearn@sandia.gov

Received 21 July 2023; revised 12 September 2023; accepted 13 September 2023; posted 14 September 2023; published 2 October 2023

**The development of atmospheric hypersonic flight and re-entry capabilities requires the characterization of the thermo-chemical state of representative test environments. This study demonstrates the usage of multiplex nanosecond $N_2$ coherent anti-Stokes Raman scattering (CARS) to measure temperatures in an atmospheric, high-temperature (>6000 K), air plasma plume, generated by an inductively coupled plasma torch. These are some of the highest temperatures ever accessed via gas-phase CARS, to our knowledge. Temperatures of $N_2$ in the equilibrium plasma plume are determined via theoretical fits to measured CARS spectra. We discuss the practical implementation of CARS at very high temperatures, including the scaling of the $N_2$ CARS signal strength from 300 to 6700 K, where the expected peak signal from the high-temperature plasma torch gases is two orders of magnitude less than commonly encountered in combustion environments. An intensified CCD camera enables single-laser-shot detection at temperatures as high as 6200 K, by increasing sensitivity and providing a time gate against intense background luminosity. We also discuss the impacts of unwanted two-beam CARS contributions from outside the nominal three-beam measurement volume. We present mean axial and radial temperature profiles, as well as time-series data derived from both single-laser-shot and accumulated CARS spectra. The single-laser-shot precision is 1.7%–2.6% at temperatures of 3500 to 6200 K. The presented results pave the way for the use of CARS at very high temperatures and the measurement of spatially resolved interface processes in high-enthalpy flows.** 

https://doi.org/10.1364/AO.501326

## 1. INTRODUCTION

The continuous development of hypersonic flight systems requires testing at high enthalpies representative of flight conditions. New heat shield materials have to be tested, and validation data are needed for better thermo-chemo-physical models. However, measurements in hypersonic flows are challenging due to high temperatures, high flow speeds, and strong background radiation.

Most materials cannot sustain high-enthalpy flow environments for very long without active cooling. Thus, intrusive measurement techniques are of limited use and can provide only limited insight. Non-intrusive, optical techniques solve this issue, but can suffer from poor sensitivity, spectral interference, and low signal-to-noise ratio (SNR). Emission spectroscopy can measure temperatures and excited species number densities, but it is a line-of-sight integrated technique dependent on natural photon emissions. Spontaneous Raman scattering can measure spatially resolved temperatures and species, but the collected signal is very weak. Coherent anti-Stokes Raman scattering (CARS) is a nonlinear optical laser diagnostic [1] that can overcome these issues. During the measurement, CARS generates a directional coherent signal beam, so that nearly the entire signal can be collected with lens and mirror arrangements. This enables spatially and temporally resolved temperature and species concentration measurements at extreme temperatures and in situations with very high background luminosity. CARS is an accurate measurement technique [1,2], has been used to detect multiple species simultaneously [3–7], and has been shown to characterize non-equilibrium states [8,9].

CARS measurements have also been performed in high-temperature flows and hypersonic test facilities. Bornemann *et al.* [10] measured the rotational and vibrational temperatures and the density of pure hydrogen in a transient filamentary discharge, yielding a peak rotational temperature of 5685 K. The spatial extent of the discharge was limited to a small volume, with rough dimensions of $10.5 \times 4\ \text{mm}^2$, and a multiplex CARS system was used, enabling single-shot measurement

of the full $H_2$ CARS spectrum. Grisch *et al.* [11] performed measurements in the arc-heated wind tunnel L2K at DLR Cologne. Their CARS system utilized a narrow-band Stokes beam, requiring scanning of the $N_2$ spectrum. Peak temperatures were measured to be around 4408 K, and they identified differences between rotational and vibrational temperatures at some measurement locations. Gülhan *et al.* [12] performed tests with a multiplex CARS system in air, using the DLR L3K arc-heated windtunnel, resulting in temperatures of about 5400 K. Due to experimental limitations, the $v = 0$ bandhead had to be partially suppressed in their temperature evaluation. Dedic *et al.* [9] used a hybrid femtosecond/picosecond CARS system to perform single-shot measurements of rotational and vibrational temperatures in a transient dielectric barrier discharge flowing a nitrogen/helium mixture. Their results exhibited strong non-equilibrium and vibrational temperatures up to 5000 K.

In this paper, we perform multiplex nanosecond CARS measurements in the subsonic plume of the UT Austin 50 kW Inductively-Coupled Plasma Torch (ICP) Facility running on dry air at atmospheric pressure. Such facilities, despite being subsonic, can replicate the flow conditions occurring behind the bow shocks of hypersonic vehicles [13]. Specifically, our facility simulates Mach 22 flight at an altitude of 45 km, based on the local heat transfer simulation methodology [13], and provides a chemically clean approach flow, because it is electrodeless. Using nanosecond CARS, we determine the $N_2$ ground state vibrational equilibrium temperature, finding peak values above 6000 K and good agreement between measurements and rotational–vibrational equilibrium fits. We report single-shot- and time-averaged temperature measurement capabilities, analyze time-series, and explore sources of uncertainty.

## 2. METHODOLOGY

### A. Experimental Setup

A picture and schematic of the UT Austin 50 kW ICP torch is shown in Fig. 1. Figure 1(a) shows a true color image of the ICP torch operating on air as the supply gas; the plasma is primarily generated inside the induction coils and then exhausts through the nozzle on top. Figure 1(b) shows a cutaway of the torch body, revealing the internal flow path geometry with the gas being injected tangentially at the bottom and then flowing up to the nozzle. The torch uses the oscillating magnetic field within the induction coil to couple energy into the partially ionized gas, resulting in a very clean plasma flow because the electrodes are not in contact with the gas. The oscillations are driven by a 6 MHz high-power radio-frequency oscillator circuit, connected to a high-voltage DC power supply. The nozzle exit diameter of the torch is 30 mm. The plasma generation is initiated with argon and then switched to air. All experiments presented here are conducted at ∼42 kW supply power, an air flow rate of 30 slpm, and an approximate bulk enthalpy of 12.5 MJ/kg. The plasma plume, which has a peak velocity of about 15 m/s, exhausts into ambient air, and Gardon gauge measurements taken 20 mm above the torch nozzle exit indicate a heat flux of 130 $W/cm^2$.

From previous Raman and emission spectroscopy measurements [14,15], we expect a plasma plume temperature around

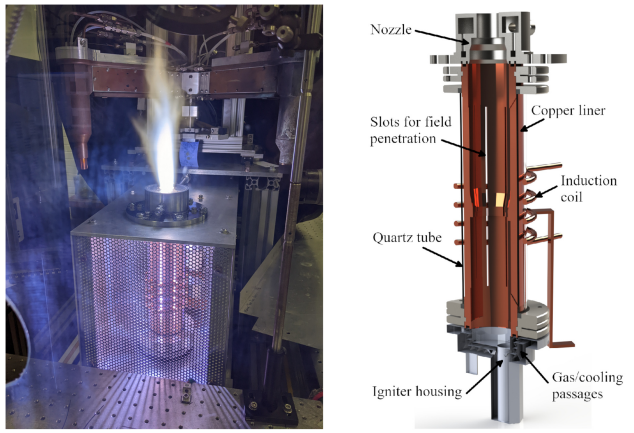


**Fig. 1.** Left: real color image of the ICP torch during a run at nominal experimental conditions. CARS measurements are performed in the plume exiting the nozzle on the top. Right: CAD model of the torch body in which the plasma is created before flowing out through the nozzle on top.

6000 K on the centerline 5–10 mm above the torch exit. About 7 mm from the centerline in the radial direction, the temperature should drop to 5000 K. We do not expect a significant degree of thermal non-equilibrium, as the average flow time from the point of plasma generation to the plume is on the order of 10 ms, whereas internal energy transfer and chemical processes for air at one atmosphere pressure and temperatures approaching 5000 K are on the order of nano- to microseconds [16]. The previous measurements [14,15] support this assertion, showing that the rotational, vibrational, and electronic temperatures are well defined by Boltzmann distributions and equal.

Measurements are performed with a nanosecond multiplex CARS system of the type described in many early CARS investigations [17–21]. A schematic of the full CARS setup is shown in Fig. 2. The CARS pump beams are frequency degenerate and derived from the 532 nm frequency doubled output of a 10 Hz pulsed Nd:YAG laser. The Nd:YAG laser pulse duration is ∼8 ns, and the laser is injection seeded to provide a narrow spectral linewidth. Manufacturer specifications state a linewidth of 0.003 $cm^{-1}$, which is consistent with measurements made using a HighFinesse WS6-200 wavemeter, showing that the laser linewidth is smaller than 0.013 $cm^{-1}$. A portion of the 532 nm laser output is used to pump a broadband dye laser consisting of Bethune-prism dye cells [22] in both the oscillator and single-pass amplifier stages. Both oscillator and amplifier

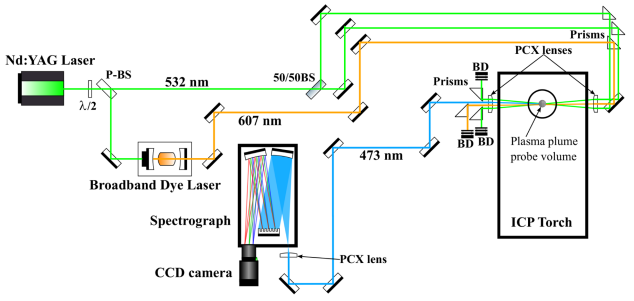


**Fig. 2.** Schematic of the CARS setup. P-BS, polarizing beam-splitter; PCX, plano–convex lens; BD, beam dumps.

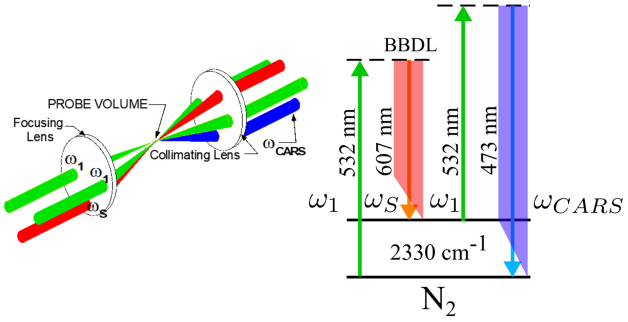


**Fig. 3.** BOXCARS beam geometry for phase matching and transition diagram for $N_2$ measurements using a broadband multiplex system.

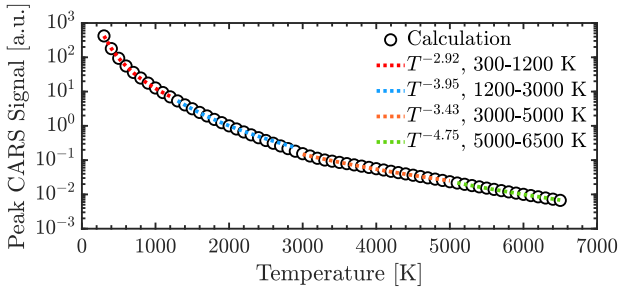


**Fig. 4.** Temperature-dependent scaling of the peak CARS signal strength. Circles represent the peak value in the CARS spectrum calculated from Eq. (1). The dashed curves indicate power-law fits to different temperature ranges, as described in the figure legend.

contain mixtures of Rhodamine 610 and Rhodamine 640 dyes, which are concentrations tuned to center the Stokes beam spectrum near 607 nm, with a spectral full-width at half-maximum (FWHM) of ∼160 $cm^{-1}$. Pulse energies are measured just ahead of the first set of turning prisms, prior to the beam-crossing lens, and these energies are mentioned for each data set in the Section 3 of this work.

At the measurement location of interest, the pump, Stokes, and probe beams are crossed in a folded BOXCARS configuration [23]; see Fig. 3. In this study, we use two different pairs of two inch (50.8 mm) diameter plano–convex lenses to form the CARS probe volume: 500 and 300 mm focal length lenses. Based on measurements with a beam profiler (DataRay WinCamD-LCM), with the 500 mm lenses, the focused pump beam diameters are ∼63 μm and the Stokes beam diameter is ∼85 μm; with the 300 mm lenses, the pump beam diameters are ∼56 μm and the Stokes beam is ∼76 μm. The diameter is derived from the area of pixels above 13.5% relative intensity.

The probe volume length could vary slightly between experiments, and nominal values are mentioned in Section 3 for each data set individually. The exact position and length of the CARS probe volume are determined using the method described by Dennis *et al.* [24]. The non-resonant CARS signal generated in a 130 − 170 μm thick microscope cover slip is recorded as the glass is translated along the axis of the beam-crossing region. The CARS signal strength is plotted versus glass-slide position, and the measurement volume center is taken as the peak of a Gaussian curve fitted to this distribution. Cumulative generation of the CARS signal is determined by integrating this signal-versus-position curve, and the axial extent of the CARS volume is taken as the region between the 5% and 95% cumulative signal points.

The CARS signal is spatially isolated from the pump and Stokes beams, which are diverted into beam dumps. Residual pump and Stokes light is removed by a series of dielectric mirrors that provide high reflectivity at the 473 nm CARS signal wavelength, while remaining transmissive to 532 and 607 nm pump and Stokes light. An interference filter effectively removes any remaining laser light and the CARS beam is dispersed by a 0.75 m grating spectrograph, employing an 1800 grooves/mm grating with 500 nm blaze. The CARS signal is dispersed onto an intensified CCD detector at 1 $cm^{-1}$ resolving power and 0.35 $cm^{-1}$/pixel dispersion.

Modern CARS investigations of this type mostly utilize low-noise backside-illuminated CCD or electron multiplying CCD detectors without image intensification. We adapted an intensified CCD in this work for multiple reasons. Time gating is required to reject the intense background plasma emissions at the 473 nm CARS wavelength. Initial tests have shown that a 10 μs is sufficient to minimize background emission; however, the intensifier gate is set to 50 ns for the majority of the experiments reported here. Second, $N_2$ CARS signal strengths from the 6000 K plasma torch plume present a challenge. Peak CARS signals exhibit a highly nonlinear dependence on temperature, arising from the well-known proportionality between the spectrally integrated CARS intensity and the square of the molecular number density, and the partitioning of this integrated signal among an increasing number of populated ro-vibrational states at high temperature. This temperature-dependent scaling of the CARS signal strength is displayed in Fig. 4, where the peak intensity in the $N_2$ Q-branch spectrum has been calculated from our CARS spectral analysis code, discussed in Section 2.B. The signal strength has been calculated for a fixed $N_2$ concentration and the results have been normalized to the value at $T = 2400$ K, approximately the adiabatic flame temperature for $H_2$/air combustion. Piecewise power-law fits to the calculated signal reveal a strong nonlinear dependence on temperature, with a $T^{-2.93}$ scaling observed at low temperatures and an even more substantial $T^{-4.75}$ dependence observed for $T = 5000 - 6500$ K. Relative to typical CARS applications in flames, the signal strength is expected to be ∼2 orders of magnitude lower in the ICP torch plume. The Gen-III intensifier used in this work had a photocathode quantum efficiency of over 50% at 473 nm and provided an estimated relative gain of one to 68, which enhanced the sensitivity of our CARS instrument for high-temperature plasma torch thermometry. Single-laser-shot sensitivity is possible, although we present results for both single-shot and shot-accumulated CARS spectra, where the intensifier is strobed in 50 ns gate intervals

### B. Data Evaluation

The CARS spectra are first background subtracted and then normalized by the non-resonant background spectrum measured in pure argon (aNRB) to correct for the finite dye laser bandwidth and spectral response of the collection system.

Temperatures are determined by fitting the corrected experimental data to a library of theoretical CARS spectra, computed with a MATLAB implementation of the Yuratich formalism [25] and assuming rotational and vibrational populations following a Boltzmann distribution with a single equilibrium temperature. The third-order susceptibility of the CARS process is

$$\chi^{(3)} \propto \alpha + \sum_{v,J} \frac{\Delta\rho_{v,J}\,(\mathrm{d}\sigma/\mathrm{d}\Omega)_{v,J}}{\omega_{v,J} - (\omega_1 - \omega_2) - i\Gamma_J/2}, \tag{1}$$

where $\alpha$ is a fitting parameter that accounts for the magnitude of the non-resonant susceptibility of the high-temperature gas mixture. The isolated line approximation is used in the Raman-resonant term, where the sum is taken over all thermally populated vibrational, $v$, and rotational, $J$, levels in $N_2$. The Raman cross section is $(\mathrm{d}\sigma/\mathrm{d}\Omega)$ computed from expressions found in Lucht *et al.* [19]. $\Delta\rho_{v,J}$ is the Boltzmann population difference, computed for each pair of energy levels coupled by Raman transitions, where we consider Q-, O-, and S-branch resonances in the sum in Eq. (1). The Raman frequencies are indicated by $\omega_{v,J}$, and $(\omega_1 - \omega_2)$ is the pump/Stokes frequency difference. The $J$-dependent Raman linewidths, $\Gamma_J$ (FWHM), are computed using the widely utilized modified exponential gap (MEG) model, with parameters for $N_2$ self-broadened Raman linewidths taken from Lavorel *et al.* [26]. The susceptibility in Eq. (1) is separately convolved with the CARS pump laser spectrum and a Gaussian slit function of 1.4 $\mathrm{cm}^{-1}$ (FWHM) to account for the resolution of our detection system. The injection-seeded pump linewidth was taken at the transform-limited value of ~0.003 $\mathrm{cm}^{-1}$, which is 8–11 times smaller than Raman linewidths at $T = 6000$ K, and has a negligible impact on the calculations.

Some approximations are made regarding the line broadening mechanisms used in this work. Foreign-gas broadening of the $N_2$ resonances is neglected. From equilibrium calculations [27] in the expected temperature range (300 to 6000 K), $N_2$ represents: 50%–78% of the total population, and remains by far the major component of the gas mixture in the plasma torch plume. Other major species populations include NO (0%–5%), atomic O (0%–32%), and $O_2$ (<1% − 21%). The MEG model for collisional Raman linewidths of $N_2$ was developed using measurements spanning from room temperature up to $T = 2400$ K [26] for rotational quantum numbers, $J$, up to ~22. This model was necessarily extrapolated to temperatures in excess of 6000 K and $J$ up to 105. At $T = 3000$ to 6000 K, the temperature-dependent change in the linewidths is weak at all $J$ and is generally 2% or less for $J$ up to 105. The $J$-dependent shape of the linewidth curve at temperatures over 3000 K additionally remains similar to that observed at lower temperatures [26,28].

Doppler broadening becomes significant at the highest temperatures encountered in the plume. At 6000 K, the Doppler width in $N_2$ is ~0.0244 $\mathrm{cm}^{-1}$, which is 7%–62% larger than the MEG-calculated Q-branch collision widths, in the range $J = 0 - 105$. The measured spectral shape is probably still dominated by the instrument function of the camera and spectrometer. Nonetheless, the impact of Doppler broadening is quantified at $T = 6000$ K using calculations from the Sandia CARSFT code [29] as a reference. The CARSFT code employs both Voigt [30] and Galatry [31] lineshapes when Doppler and collisional effects become comparable. A fit of our isolated-line model to an $N_2$ spectrum, calculated using Voigt lineshapes by CARSFT, is shown in Fig. 5. Our model employs molecular parameters and self-broadened collisional linewidths for $N_2$ identical to CARSFT. Fitting parameters include the temperature and the non-resonant scaling factor, $\alpha$ in Eq. (1). The fitted temperature is $T_{\mathrm{fit}} = 6066$ K, within 1.1% of the 6000 K value used in the CARSFT calculation. This high-temperature case represents the worst case, since Doppler broadening is reduced at lower temperatures. Thus, based on the level of agreement, we feel that the isolated line remains a reasonable approximation for $N_2$ under the very high temperatures encountered in the plasma torch plume, which saves us considerable time in data processing.

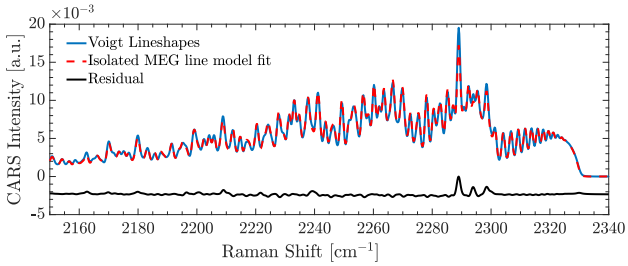


**Fig. 5.** Comparison of our MATLAB code, using the isolated line MEG model, to a CARSFT spectrum using Doppler broadened Voigt line profiles. The CARSFT spectrum is used as a reference and the MATLAB spectrum is fitted to it. The CARSFT spectrum is calculated for $T = 6000$ K and $\alpha = 0.005$, and the MATLAB fit yields $T_{\mathrm{fit}} = 6023$ K and $\alpha_{\mathrm{fit}} = 0.002$.

## 3. RESULTS

We present practical considerations for CARS measurements at very high temperatures, representative spectra, and temperature time-series. We show axial and radial temperature profiles in the ICP torch, obtained with two different sets of probe volume forming lenses. Finally, we assess the precision in our CARS derived temperatures, based on both single-laser-shot and shot-accumulated spectra, and provide uncertainty bounds.

### A. Practical Considerations at High Temperatures

Two effects that can deteriorate the accuracy of CARS measurements are unwanted two-beam interaction (2BI) and stimulated Raman pumping (SRP). We will first consider unwanted 2BI, which is generated through the interaction of a single pump beam with the Stokes source, achieving a four-wave mixing process. This interaction occurs at a small crossing angle, over an extended length away from the focused beam waists. The 2BI signal propagates collinearly with the pump beam and, if not properly filtered, can pollute the proper CARS measurement with a signal generated outside the nominal probe volume, where the desired three-beam CARS process occurs. 2BI is of particular concern when the Stokes beam focus is poor, i.e., the beam quality is low, and when the signal level for the desired three-beam process is low, as per Fig. 4.

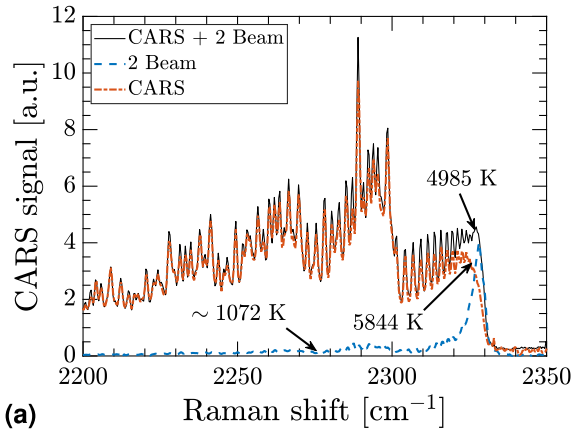


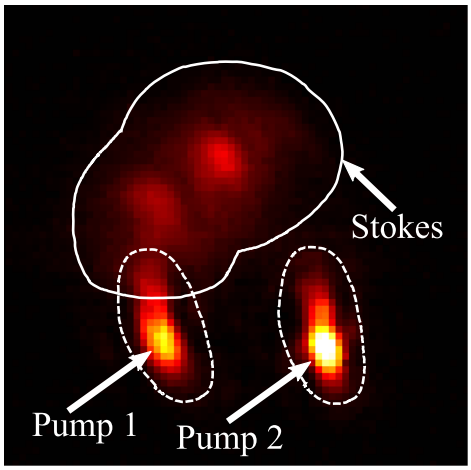


**Fig. 6.** Data showing the origin and effect of the 2BI. Spectra are averaged from 50 measurements, each consisting of an accumulation of 10 shots, taken with 28 mJ/pulse and 32 mJ/pulse in the pump beams, and 19 mJ/pulse in the Stokes beam. The probe volume is formed with 500 mm focal length convex lenses. (a) Gain normalized data illustrating the effect of two-beam interaction on recorded CARS spectra. The gain is set to 49, in all cases. (b) Beam image 7.6 mm ahead of the nominal beam crossing. The low-quality Stokes beam is defocusing more severely than the pump beams.

Using a beam-profiling camera, we visualized the beam arrangement away from the nominal probe volume in an early version of our setup; see Fig. 6(b). While the pump beams are still relatively well focused, the Stokes beam diverges quickly and exhibits two intensity lobes, one of which is partially overlapped with the "Pump 1" beam and can generate a signal away from the desired three-beam measurement volume. Larger beam sizes encountered away from the beam waist can result in very long two-beam interaction lengths, contributing to a CARS signal that propagates collinearly with the pump beam. This nuisance CARS signal can be mitigated by improving the Stokes beam focus quality, which we accomplished by spatially restricting the beam with an aperture, or by using a shorter focal length probe volume forming lens, to increase the crossing angle. Additionally, the 2BI contribution is only partially overlapped with the three-beam BOXCARS signal in space and can be further minimized by a tight aperture in the collection optics.

2BI is particularly concerning when measurements are performed in a steep temperature gradient, with the measurement volume in a hot region, surrounded by much colder gases, as, for example, in the plasma torch plume. 2BI is similar to the well-known spatial averaging effect present along the three-beam CARS focal volumes [32–34]. Peak CARS signal strengths exhibit a strong, nonlinear dependence on temperature ($T^{-3} - T^{-5}$ per Fig. 4), and on beam-overlap length ($l^2$) [1]. Thus, contributions from significantly colder gas in regions of long, weakly focused beam overlap may become comparable to the desired, but weak, three-beam CARS interaction in the hot gas. The resulting CARS spectra may then exhibit a bias toward low-temperature regions. In low-gradient flows, 2BI signals will be weak compared to the desired three-beam contribution but these nuisance contributions can become significant in the plasma torch plume, where changes in temperature of over 4000 K are present in the radial temperature profile across the ~30 mm diameter of the plume.

The 2BI effect is illustrated in Fig. 6(a), where multiple CARS measurements are shown, with the measurement volume positioned on the centerline of the plasma plume, 6 mm above the nozzle exit. The CARS spectra are normalized by their corresponding gain setting. The "CARS + 2-Beam" result is the desired three-beam CARS spectrum biased by an unwanted 2BI signal from much colder gas. This measured spectrum was fit to a temperature of $T = 4985$ K. The desired three-beam CARS spectrum was recovered by aperturing the Stokes beam spatial profile to improve its quality; this desired spectrum is indicated as "CARS" in Fig. 6(a) and was fit to a temperature of 5844 K, 17% higher than the temperature obtained from the 2BI-contaminated spectrum. The 2BI contribution to the signal was isolated by blocking the central portion of the CARS signal beam to recover the "2-Beam" spectrum in Fig. 6(a), which displayed a much narrower width in the $v = 0$ spectrum, with little hot-band contributions from higher vibrational states, and was fit to a very low temperature of ~1072 K. Even though the 2BI signal was weak, it clearly distorted the desired three-beam CARS signal, and the change in the vibrational $v = 0$ bandhead yielded lower temperatures, as indicated in Fig. 6(a). Interestingly, the rest of the CARS + 2-beam spectrum and the non-resonant background appear unaffected. The bias towards lower temperatures seems to be entirely caused by the distortion of the $v = 0$ spectrum.

The other effect that can deteriorate the accuracy of the CARS measurement is SRP. It occurs when the Raman-resonant optical field in the probe volume becomes so strong that a significant population is transferred from the lower, $v$, to the upper level, $v + 1$, coupled by the Raman process on the ~8 ns time scale of the laser pulses. The CARS spectra may then reflect an artificially high temperature due to the movement of vibrational population during the laser pulse [35,36]. We evaluated the pulse-energy dependence of our CARS spectra in the 6000 K torch interior and limited the fluence levels to the values in Table 1. With these fluences, no discernible SRP is observed, and the time scale over which the Raman process transfers population is above the threshold defined by Woodmansee *et al.* [36].

**Table 1. Properties of the CARS Setup for Different Data Sets[a]**

| Profile Type | Lenses | $L$ [mm] | Pumps [mJ]\|[GW/cm$^2$] | Stokes [mJ]\|[GW/cm$^2$] |
|---|---|---|---|---|
| Axial | 500 mm | 3.0 | 28/32 \| 111/127 | 19 \| 42 |
| Axial | 300 mm | 1.7 | 13/22 \| 67/114 | 13 \| 36 |
| Radial | 500 mm | 3.1 | 28/32 \| 111/127 | 19 \| 42 |
| Radial | 300 mm | 1.7 | 13/22 \| 67/114 | 13 \| 36 |

[a]Pumps and Stokes refer to the pump and Stokes beams. $L$ is the 5%–95% length of the CARS probe volume.

### B. CARS Spectra and Temperature Profiles

Representative examples of fits to a 500-shot-averaged CARS spectrum, a 10-shot average, and to a single-laser-shot spectrum are shown in Fig. 7. These data were acquired on the jet centerline, 6 mm above the torch nozzle exit, where temperatures approached 6000 K. A 300 mm focal length beam-crossing lens was used, with a measured three-beam overlap length of 1.7 mm. The measurements were taken at pulse energies of 13 and 22 mJ/pulse in the pump beams, and 13 mJ/pulse in the Stokes beam. The 500-shot average in Fig. 7(a) corresponds to 50 s of measurement time at 10 Hz, which minimizes noise contributions from Stokes dye laser fluctuations [37]. The resulting CARS spectrum is quite complex, with contributions from five overlapping ro-vibrational bands. The corresponding fit using the standard CARS model described in Section 2.B remains of reasonable quality at the extreme $T = 6144$ K result. The 10-shot average in Fig. 7(b) corresponds to 1 s of measurement time, and the residual is slightly more noisy, but the signal-to-noise ratio in the data appears reasonable. Single-laser-shot spectra were attainable, even at this extreme temperature and a modest 1.7 mm probe volume length. The signal-to-noise is notably decreased in the single-shot results, but the fit temperature is still in reasonable agreement (1%–2.5%) with the shot-averaged temperatures, likely as a result of the significant, temperature sensitive hot-band structure in the data. Furthermore, the overall good agreement between the fits and the experimental data indeed suggests that the plasma plume is in thermal equilibrium as expected. Otherwise, we would expect to see significant systematic deviations from the theoretical single temperature spectra utilized here, necessitating a more involved data evaluation, e.g., utilizing a multi-temperature model.

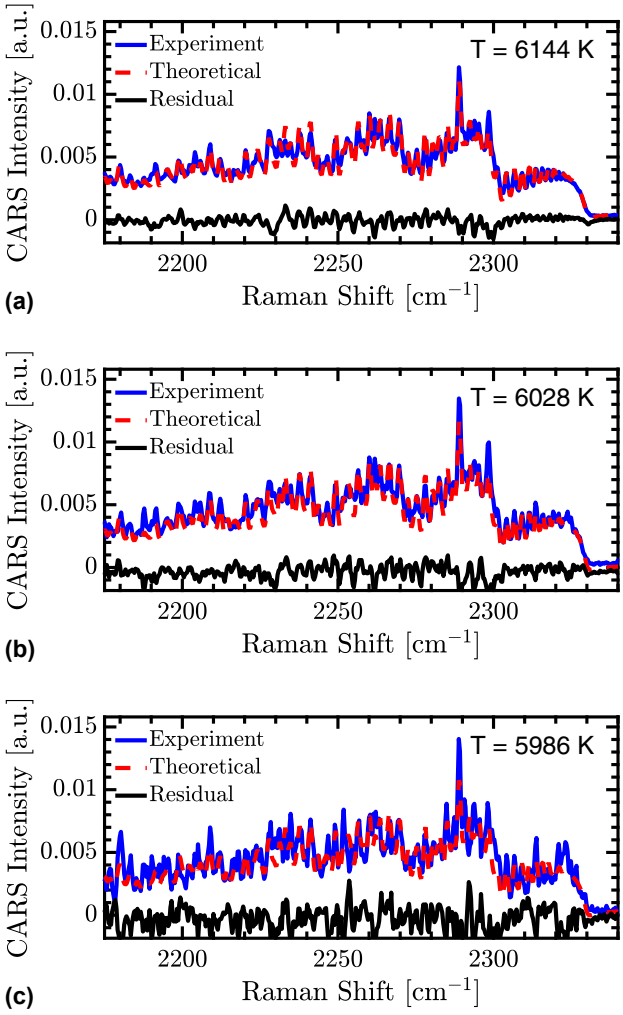


**Fig. 7.** Example spectra and MATLAB fits for measurements taken on the centerline 6 mm above the nozzle using the $f = 300$ mm beam-crossing lenses to form the probe volume. The average spectrum is the mean of 500 single shots. The single-shot spectrum is a representative example from this data set. (a) 500-shot average spectrum, (b) 10-shot average, and (c) single-shot.

Time-mean temperature profiles taken in the air plasma plume of the ICP torch are shown in Fig. 8. We took data sets at an air flow rate of 30 slpm and ∼42 kW input power, with 300 and 500 mm beam-crossing lenses deployed in repeat experiments. Probe volume lengths and beam energies are given in Table 1. Care was taken to mitigate the aforementioned effects of 2BI and SRP. The data acquired with 300 mm lenses consist only of single-laser-shot results. For the 500 mm lens measurements, the on-chip accumulation was adjusted between one and 10 shots at a given measurement point to yield the best SNR.

The axial temperature profile along the centerline of the ICP torch plume is shown in Fig. 8(a). The temperature decreases monotonically and smoothly, as one would expect for a hot buoyant jet. Temperatures obtained using both 300 and 500 mm lenses generally agree within 5%. The mean temperatures derived from averaged spectra are up to 19% lower than the values derived from the average of single-laser-shot temperatures. This, again, is a result of the strong nonlinear dependence of CARS intensities on temperature, as per Fig. 4. Beyond about $\sim 50 - 60$ mm downstream of the nozzle exit, the temperature measurements start to diverge more notably. At this point, entrainment of cold ambient air becomes relevant. Due to dynamic range limitations, the intensified CCD camera saturated when the measured region became too cold, especially when signal was accumulated on the CCD chip for multiple laser shots. Saturated measurements have to be discarded, and, thus, the averaged results are biased towards higher temperatures. The longer probe volume data are more strongly affected by the dynamic range limitation, because we accumulated signals on the chip in this case. At most, 20% of the samples had to be rejected using the 500 mm lens pair for data acquired beyond 50 mm from the nozzle exit, whereas only a maximum of 3% of single-laser-shot spectra had to be rejected when using the 300 mm beam-crossing lenses. The average rejection rate

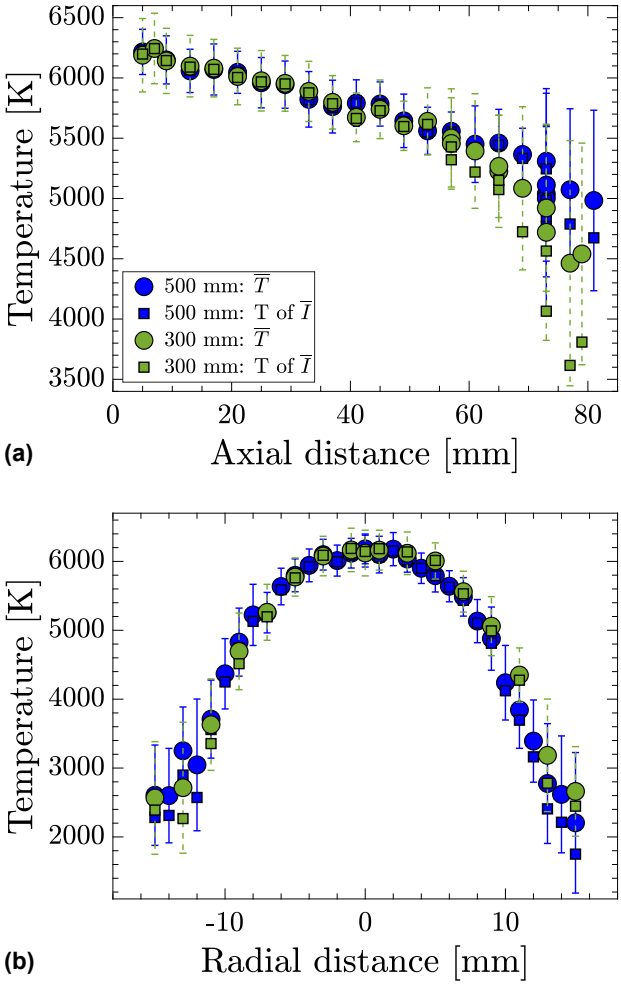


**Fig. 8.** Mean temperature profiles taken in the ICP torch. Circles are data taken with 500 mm lenses, squares with 300 mm lenses. Blue data points represent an average of CARS temperature time-series obtained from single-laser-shot (300 mm lens) or several on-chip accumulations (500 mm lens). Green data points represent temperatures obtained by fitting a single long-time-averaged CARS spectrum. Error bars represent uncertainty in the blue data points. (a) Axial temperature profile. (b) Radial temperature profile 6 mm above the nozzle exit.

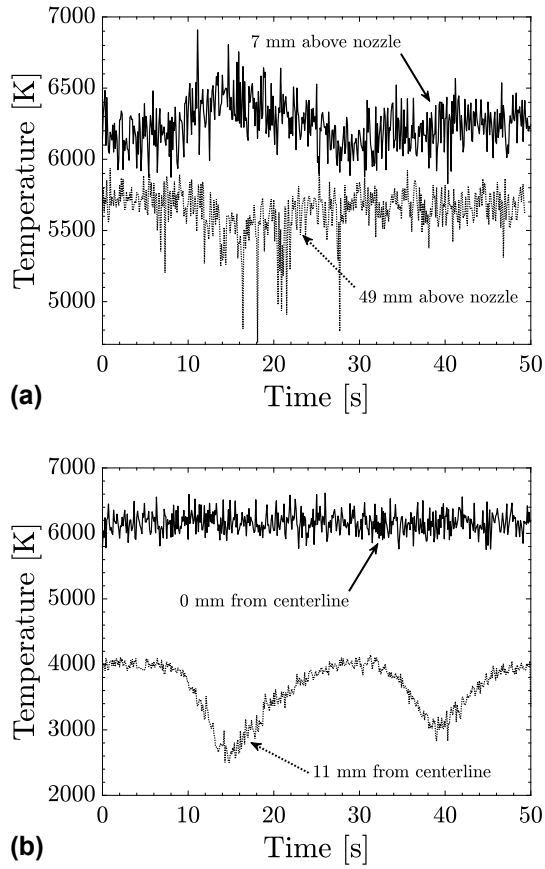


**Fig. 9.** Temperature time-series from single-laser-shot data: 500 single shots over a 50 s observation time using the 300 mm beam-crossing lenses. (a) Time-series from measurements on the centerline. (b) Time-series from measurements recorded 6 mm above the nozzle exit at the centerline and at 11 mm outward.

beyond the 50 mm mark is 2% and <1%, for the 500 and 300 mm crossing lenses, respectively.

In Fig. 8(b), we show the radial temperature profiles obtained 6 mm above the nozzle exit. Near the jet centerline, temperatures generally agree within 1% for the same averaging schemes described above. The temperature drops nearly monotonically from the center of the plume towards the edge, as one would expect for a hot axisymmetric jet. Similar to the axial profile measurements, temperatures obtained from fits to averaged spectra are up to 21% lower than the average of single-laser-shot temperatures at the edges of the plume, where cold-gas entrainment becomes increasingly likely, resulting in increased levels of disagreement between 500 and 300 mm lens pair conditions. Spatial averaging effects due to large temperature gradients at the edge of the plume [33,34,38] were estimated to be negligible, as we explain further in Section 3.D.

### C. Temperature Time-Series

Time-series of 500 single-laser-shot CARS temperatures are shown in Fig. 9. Measurements obtained on the jet centerline at heights of 7 and 49 mm above the nozzle exit, using a 300 mm beam-crossing lens, are shown in Fig. 9(a), while data acquired 6 mm above the nozzle on the centerline and 11 mm radially outward with 500 mm lenses are displayed in Fig. 9(b). The three time-series acquired on the centerline display maximum excursions of ∼500 K, with high-frequency fluctuations of order ±250 K. At 11 mm from the centerline, closer to the jet shear layer, the temperature history displays a nearly periodic variation, with a period close to 25 s, and a large temperature excursion from 2600 to 4000 K. This kind of long-time-scale fluctuation can also be seen on the jet centerline when the data are sampled for a much longer time interval, as in Fig. 10. Here we present CARS temperatures from the jet centerline at 6 mm above the nozzle, over a much longer, 300 s, data window. These centerline time-series data exhibit mean and rms fluctuating temperature values of $6154 \pm 113$ K and $6229 \pm 105$ K, obtained using 500 and 300 mm CARS beam-crossing lenses, respectively.

We believe that the observed long-time-scale temperature fluctuations are the result of aliasing and represent real temperature fluctuations, not measurement error. Observation of

single-laser-shot non-resonant CARS spectra acquired in argon over a sampling window of several minutes revealed no systematic variation in center frequency or bandwidth, which would be the most likely error-based cause of long-time drift in our CARS temperatures. Previous characterization of this plasma torch facility showed 180 Hz fluctuations in plume luminosity [15], which result from imperfect rectification of the 60 Hz AC line frequency, as previously reported for other inductively coupled plasma flow facilities [39,40]. Downsampling of plume luminosity data to the 10 Hz Nd:YAG laser repetition rate revealed aliased low-frequency content near 0.05 Hz, consistent with the observed ∼20 s period, in particular at $r = 11$ mm in Fig. 9(b). Sampling of the plume luminosity data to non-integer multiples of 180 Hz randomizes the low-frequency content.

### D. Measurement Precision and Accuracy

The precision in our CARS temperature data was estimated for both the time-series results shown in Section 3.C and for the mean temperatures in Fig. 8. We believe that frequency content below 0.067 Hz (15 s period) represents real, but aliased, temperature fluctuations, while noise associated with the CARS measurements is represented by uncorrelated high-frequency temperature fluctuations. We assessed the precision of time-series data within the interior of the plume, where cold-gas entrainment was insignificant. In Fig. 8, this corresponds to jet centerline measurement stations up to $z = 55$ mm from the nozzle exit and radial locations within ±11 mm from the centerline at $z = 6$ mm. Both shot-accumulated and single-laser-shot results were considered. The time-series temperatures in Fig. 10 represent 10-shot-accumulated results. After removal of the low-frequency content below 0.067 Hz using Fourier filtering, the standard deviation of these long-duration time-series is $\sigma_T = \pm 113$ and 105 K, respectively, for 500 and 300 mm beam-crossing lenses, or ∼1.8% of the mean temperatures of 6154 and 6229 K. A similar level of precision of ∼1% is observed for shot-accumulated time-series from the high-temperature interior of the plume using the 500 mm beam-crossing lenses.

Single-laser-shot precision was also evaluated after removal of low-frequency content, using CARS spectra acquired with 300 mm beam-crossing lenses (e.g., using data such as shown in Fig. 9). The single-shot standard deviation is 1.7%–2.6% of the mean temperature for $\bar{T} > 3500$ K; see, for example, Fig. 11. The best level of precision is encountered around temperatures of $\bar{T} \sim 4000 - 5800$ K, with $\sigma_T/\bar{T} \sim 1.7\%$. This level of single-shot precision compares favorably with previous reports of $N_2$ vibrational CARS thermometry at flame temperatures using single-mode pump lasers and a multimode Stokes dye source, where measurement precision is ∼3% − 5% [41–43]. The 1.7% precision observed near the jet centerline at

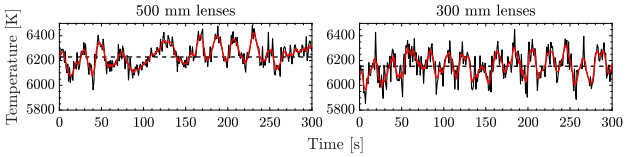


**Fig. 10.** 300 s window of temperature time-series collected over 900 s, 6 mm above the nozzle on the jet centerline. Black lines are the temperature series, red lines are moving averages with window length five, and dashed lines are the average temperatures.

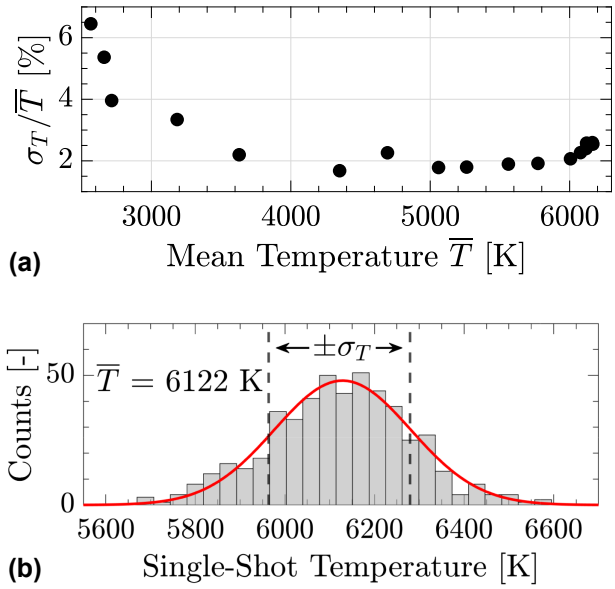


**Fig. 11.** Analysis of the relative precision of single-shot temperature measurements using data in Fig. 8(b) obtained with the 300 mm beam-crossing lenses. (a) Relative precision as a function of mean temperature. (b) Histogram of single-shot temperatures measured in the center of the plume at $r = 0$ mm. The red line is a Gaussian fit to the histogram data.

$\bar{T} \sim 5000$ K is comparable to some of the best reported values obtained with femtosecond pump and Stokes sources [44–46], whose transform-limited performance is far superior to noisy multimode dye lasers. It is possible that the robust details offered by four to five detectable vibrational bands combined with the well-resolved rotational structure in our CARS spectra result in enhanced precision at high temperatures. Nonetheless, as the temperature keeps increasing towards the center of the plume and the peak CARS signal keeps decreasing (see Fig. 4), eventually, the gain in precision due to more spectral details seems to be outweighed by the decreasing SNR, explaining the lower relative precision at temperatures >5800 K in Fig. 11(a).

The precision in the mean temperature data of Fig. 8 is impacted both by the random scatter in the underlying CARS time-series results and by the low-frequency content with $\sim 15 - 25$ s periods, which leads to sampling errors for the finite 50 s record lengths employed. We estimated the precision of the mean temperatures from the sample variance of the underlying 50 s time-series records. For statistically independent samples, the mean temperature exhibits a variance $\sigma_T^2/N$, where $N$ is the number of independent samples, and $\sigma^2$ is the variance of the time-series data. However, the 50 s record length represents at most 2.5 correlation times, reflecting the sampling error. Therefore, random error in the mean temperatures was estimated from the student's t-distribution; see the first term on the RHS of Eq. (2), where $\beta$ represents the fraction of time-series samples unaffected by detector saturation and is relevant only in lower temperature regions with significant cold-gas entrainment. If $\beta = 1$, then $t \approx 2.56$, based on a ±90% confidence interval, and the total sample size is conservatively restricted to $N = 2.5$:

$$U_T^2 = t_{\alpha,\nu}^2 \frac{\sigma_T^2}{\beta \cdot 2.5} + \left(0.02 \cdot \bar{T}\right)^2. \quad (2)$$

Other potentially significant sources of measurement uncertainty for the mean temperatures include spatial "density weight" averaging [33,34,38] and uncertainty in the non-resonant background of very-high-temperature air. Low-temperature bias from spatial averaging was estimated using synthetic spectra, as done in multiple previous reports [33]. The synthetic CARS spectra were generated by assuming radial temperature profiles with a peak value of $T = 6200$ K and a shape similar to those reported in Fig. 8(b). Accumulation of CARS signal strength along the measurement volume axis was modeled by integrating a Gaussian signal strength profile over the measured 1.7 and 3.1 mm axial measurement lengths for 300 and 500 mm focal length lenses. The estimated spatial averaging error is 0.5% or less across the full radial extent of the average plume temperature profile, and this source of error has been neglected in the remainder of our analysis. This may not be particularly surprising given the excellent quantitative agreement of the radial temperature profiles in Fig. 8 for the two different measurement volume lengths.

Fitting the temperature and non-resonant background simultaneously represents an additional source of uncertainty, as temperature and non-resonant background exhibit a strong negative correlation in $N_2$ vibrational CARS spectra. Reasonable bounds for $\chi_{nr}$ of air at $T = 3000 - 6000$ K are difficult to estimate, due to a lack of information regarding the third-order non-resonant susceptibility of atomic oxygen and nitrogen. To estimate the magnitude of this potential systematic error, we used the mean and standard deviation of the $\alpha$ fitting parameter in Eq. (1) derived from the long time-series results in Fig. 10. We re-fit the corresponding CARS spectra with $\alpha$ fixed at values $+2$ and $-2$ standard deviations from the mean, corresponding to a variation in $\alpha$ of ~20%. None of the fitted values of $\alpha$ for the results in Fig. 10 falls outside this range. The resulting temperatures are within 2% of the original values obtained by varying $\alpha$ in the fit routine. Thus, we consider an additional uncertainty due to floating the $\chi_{nr}$ scaling factor as 2% of the mean temperature; see the second term on the RHS of Eq. (2). The resulting uncertainty intervals are shown as error bars in Fig. 8.

Accuracy of CARS and other laser-diagnostic measurements is most often assessed using steady, well-characterized flat flames [47,48], for which comparable sources are not presently available at the extreme temperatures encountered in this study. Fries *et al.* [15] report emission spectroscopy temperatures of 5600–5700 K at $z = 10$ mm above the nozzle for the same 10 kV and 30 slpm condition used here. These temperatures are 5%–10% lower than the 6000–6200 K CARS data, but we may expect some degree of spatial averaging to lower the emission temperature. Greene *et al.* [14] report radially resolved, Abel-inverted profiles of emission temperature at $z = 5$ mm above the torch, at an anode voltage of 10 kV, and bulk gas flow of 25 slpm. Their centerline temperature is ~5900 K, with a temperature near 5100 K at 7 mm radially outward from the jet axis, both of which compare favorably to CARS-measured values of 6000–6200 K on the jet centerline and 5000/5274 K at $r = \pm 7$ mm, respectively, in Fig. 8(b). Spontaneous Raman scattering measurements performed at 10.5 kV anode voltage, 30 slpm bulk air flow, and $z = 15$ mm above the nozzle exit indicate $T \sim 5750$ K at the jet centerline and ~4800 K at $r = 7.5$ mm [49]. These corroborating experimental data, while admittedly limited, suggest good accuracy of our high-temperature CARS data, with values generally within 100–300 K for Abel-inverted emission, Raman, and CARS measurements at temperatures near 6000 K on the near-field jet centerline.

## 4. CONCLUSION

We have presented high-quality nanosecond multiplex CARS measurement at extremely high temperatures, up to 6200 K, from the atmospheric pressure gas plume of an inductively coupled air plasma torch. Practical considerations for very-high-temperature measurements have been summarized. A Gen-III intensified CCD camera enabled these measurements by providing short, 20 ns time gates to reject intense background torch luminosity. The intensifier gain additionally boosted low CARS photon yields from the extreme-temperature gases, which resulted in two orders of magnitude reduction in signal strength relative to typical flame applications. These small CARS signals may be corrupted by weakly phase-matched, two-beam CARS processes resulting from partial pump-Stokes overlap over a much larger spatial extent than the desired three-beam CARS volume. The user must be aware of these potential nuisance signal contributions and can readily eliminate them by spatially isolating the CARS signal beam in the collection optics and/or by reducing the size of the Stokes laser beam. This two-beam interaction results in a low-temperature bias that approached ~1000 K in the example presented here.

We report CARS temperatures based on both single-laser-shot and multi-shot accumulations of $N_2$ Q-branch spectra. Temperature time-series revealed a long-duration (~20 s) quasi-periodic fluctuation, whose magnitude is ±250 K near the jet centerline and approached 1500 K at radially outward positions near the shear layer between the hot plume gases and the surrounding room air. This long-period perturbation in the jet temperatures was determined to result from aliasing of real temperature fluctuations at 180 Hz by the much lower 10 Hz repetition rate of the Nd:YAG laser. When the low-frequency content was removed from the CARS time-series, rms measurement fluctuations of 1.0%–2.6% of the mean temperature were determined in the 3500–6200 K temperature range for both single-laser-shot and 10-shot accumulations of CARS spectra. This high degree of precision is competitive with the best reported nanosecond CARS measurements using single-mode pump and multimode broadband Stokes lasers and approaches reported measurement precision obtained with transform-limited femtosecond pump/Stokes sources. One reason for this robust level of precision may be the highly detailed structure of our rotationally resolved $N_2$ CARS spectra, whose frequency content spans as many as five to six vibrational levels and 200 $cm^{-1}$ of wavenumber space.

An analysis of measurement accuracy compares the CARS temperature data to Abel-inverted emission-based and spontaneous Raman thermometry obtained in the same plasma torch facility. The three methods provide jet centerline temperatures within 100–300 K at $T \sim 6000$ K, or 1.7% to 5.0%. Spatial

averaging was negligible (0.5% or less), despite the very high radial temperature gradients present, and the radial temperature profiles exhibit agreement to better than 5% for CARS measurement volume lengths of 1.7 and 3.1 mm. Uncertainties in the non-resonant background of high-temperature air were examined and estimated to provide a 2% potential systematic error. CARS thermometry at such very high temperatures is timely, given high levels of current interest in hypersonic flight applications and plasma science. The high-temperature performance of the technique can be improved by assessing Raman linewidths in air at temperatures far in excess of flame conditions, and by robust measurement or calculation of the non-resonant susceptibilities of atomic O and N species.

**Funding.** National Nuclear Security Administration (DE-NA0003969, DE-NA0003525) U.S. Army (W911NF1920333).

**Acknowledgment.** Authors DF, SS, NC, and PV are supported by the Department of Energy, National Nuclear Security Administration. JM is supported by the US Army. RB, EJ, and SK are employed by Sandia National Laboratories, a multi-mission laboratory managed and operated by National Technology and Engineering Solutions of Sandia, LLC., a wholly owned subsidiary of Honeywell International, Inc., for the U.S. Department of Energy's National Nuclear Security. The authors thank Chris Madden and Jeremy Jagodzinsky for their support of the research work.

**Disclosures.** The authors declare no conflicts of interest.

**Data availability.** Data underlying the results presented in this paper are not publicly available at this time but may be obtained from the authors upon reasonable request.

## REFERENCES

1. A. C. Eckbreth, *Laser Diagnostics for Combustion Temperature and Species* (CRC Press, 1996), Vol. **3**.
2. S. Roy, J. R. Gord, and A. K. Patnaik, "Recent advances in coherent anti-Stokes Raman scattering spectroscopy: fundamental developments and applications in reacting flows," Prog. Energy Combust. Sci. **36**, 280–306 (2010).
3. A. C. Eckbreth and T. J. Anderson, "Dual broadband CARS for simultaneous, multiple species measurements," Appl. Opt. **24**, 2731–2736 (1985).
4. R. P. Lucht, "Three-laser coherent anti-stokes Raman scattering measurements of two species," Opt. Lett. **12**, 78–80 (1987).
5. M. P. Thariyan, V. Ananthanarayanan, A. H. Bhuiyan, S. V. Naik, J. P. Gore, and R. P. Lucht, "Dual-pump CARS temperature and major species concentration measurements in counter-flow methane flames using narrowband pump and broadband stokes lasers," Combust. Flame **157**, 1390–1399 (2010).
6. E. Gallo, L. Cantu, A. D. Cutler, M. J. Rahimi, and H. K. Chelliah, "WIDECARS measurements of major species concentration and temperature in an air-ethylene flame," *30th AIAA Aerodynamic Measurement Technology and Ground Testing Conference*, Atlanta, Georgia, USA, 2014, p. AIAA 2014-2525.
7. N. Rock, P. S. Hsu, D. Lauriola, N. Rahman, J. Estevadeordal, S. W. Grib, N. Jiang, S. P. Kearney, and P. Wrzesinski, "WIDECARS multi-parameter measurements in premixed ethylene–air flames using a wavelength stable ultrabroadband dye laser," Appl. Opt. **59**, 2649–2655 (2020).
8. W. R. Lempert and I. V. Adamovich, "Coherent anti-Stokes Raman scattering and spontaneous Raman scattering diagnostics of nonequilibrium plasmas and flows," J. Phys. D **47**, 433001 (2014).
9. C. E. Dedic, T. R. Meyer, and J. B. Michael, "Single-shot ultrafast coherent anti-Stokes Raman scattering of vibrational/rotational nonequilibrium," Optica **4**, 563–570 (2017).
10. T. Bornemann, V. Kornas, V. Schulz-von der Gathen, and H. F. Döbele, "Temperature and concentration measurements of molecular hydrogen in a filamentary discharge by coherent anti-Stokes Raman spectroscopy (CARS)," Appl. Phys. B **51**, 307–313 (1990).
11. F. Grisch, P. Bouchardy, V. Joly, C. Marmignon, U. Koch, and A. Gulhan, "Coherent anti-Stokes Raman scattering measurements and computational modeling of nonequilibrium flow," AIAA J. **38**, 1669–1675 (2000).
12. A. Gülhan, B. Esser, U. Koch, M. Fischer, E. Magens, and V. Hannemann, "Characterization of high-enthalpy-flow environment for ablation material tests using advanced diagnostics," AIAA J. **56**, 1072–1084 (2018).
13. A. F. Kolesnikov, "Extrapolation from high enthalpy tests to flight based on the concept of local heat transfer simulation," Technical report (Institute for Problems in Mechanics Moscow (USSR), 2000).
14. B. R. Greene, N. T. Clemens, P. L. Varghese, S. Bouslog, and S. V. Del Papa, "Characterization of a 50kw inductively coupled plasma torch for testing of ablative thermal protection materials," in *55th AIAA Aerospace Sciences Meeting* (2017), paper AIAA 2017-0394.
15. D. Fries, N. T. Clemens, and P. L. Varghese, "Time dynamics of an inductively coupled plasma torch," in *AIAA SciTech 2022 Forum* (2022), paper AIAA 2022-0984.
16. J. D. Anderson, *Hypersonic and High Temperature Gas Dynamics* (McGraw-Hill, 1989).
17. W. B. Roh, P. W. Schreiber, and J. P. E. Taran, "Single-pulse coherent anti-Stokes Raman scattering," Appl. Phys. Lett. **29**, 174–176 (1976).
18. J. Zheng, J. B. Snow, D. V. Murphy, A. Leipertz, R. K. Chang, and R. L. Farrow, "Experimental comparison of broadband rotational coherent anti-Stokes Raman scattering (CARS) and broadband vibrational CARS in a flame," Opt. Lett. **9**, 341–343 (1984).
19. R. P. Lucht, R. E. Palmer, and M. A. Maris, "Simultaneous acquisition of pure rotational and vibrational nitrogen spectra using three-laser coherent anti-Stokes Raman spectroscopy," Opt. Lett. **12**, 386–388 (1987).
20. M. Aldén, P.-E. Bengtsson, H. Edner, S. Kröll, and D. Nilsson, "Rotational CARS: a comparison of different techniques with emphasis on accuracy in temperature determination," Appl. Opt. **28**, 3206–3219 (1989).
21. J. Jonuscheit, A. Thumann, M. Schenk, T. Seeger, and A. Leipertz, "One-dimensional vibrational coherent anti-Stokes Raman-scattering thermometry," Opt. Lett. **21**, 1532–1534 (1996).
22. D. S. Bethune, "Dye cell design for high-power low-divergence excimer-pumped dye lasers," Appl. Opt. **20**, 1897–1899 (1981).
23. A. C. Eckbreth, "BOXCARS: crossed-beam phase-matched CARS generation in gases," Appl. Phys. Lett. **32**, 421–423 (1978).
24. C. N. Dennis, C. D. Slabaugh, I. G. Boxx, W. Meier, and R. P. Lucht, "Chirped probe pulse femtosecond coherent anti-Stokes Raman scattering thermometry at 5 KHz in a gas turbine model combustor," Proc. Combust. Inst. **35**, 3731–3738 (2015).
25. M. A. Yuratich, "Effects of laser linewidth on coherent anti-Stokes Raman spectroscopy," Mol. Phys. **38**, 625–655 (1979).
26. B. Lavorel, L. Guillot, J. Bonamy, and D. Robert, "Collisional Raman linewidths of nitrogen at high temperature (1700–2400 K)," Opt. Lett. **20**, 1189–1191 (1995).
27. S. Gordon and B. J. McBride, "Computer program for calculation of complex chemical equilibrium compositions and applications," NASA Reference Publication 1311 (1996).
28. R. L. Farrow, R. Trebino, and R. E. Palmer, "High-resolution CARS measurements of temperature profiles and pressure in a Tungsten lamp," Appl. Opt. **26**, 331–335 (1987).
29. R. E. Palmer, "The CARSFT computer code calculating coherent anti-Stokes Raman spectra: User and programmer information," Technical report (Sandia National Lab (SNL-CA), 1989).
30. J. Humlček, "An efficient method for evaluation of the complex probability function: the Voigt function and its derivatives," J. Quant. Spectrosc. Radiat. Transfer **21**, 309–313 (1979).
31. L. Galatry, "Simultaneous effect of Doppler and foreign gas broadening on spectral lines," Phys. Rev. **122**, 1218–1223 (1961).
32. J. P. Boquillon, M. Pealat, P. Bouchardy, G. Collin, P. Magre, and J. P. Taran, "Spatial averaging and multiplex coherent anti-Stokes Raman scattering temperature-measurement error," Opt. Lett. **13**, 722–724 (1988).
33. J. Y. Zhu and D. Dunn-Rankin, "CARS thermometry in high temperature gradients," Appl. Phys. B **56**, 47–55 (1993).

34. J. D. Garman and D. Dunn-Rankin, "Spatial averaging effects in CARS thermometry of a nonpremixed flame," Combust. Flame **115**, 481–486 (1998).
35. P. R. Regnier, F. Moya, and J. P. E. Taran, "Gas concentration measurement by coherent Raman anti-stokes scattering," AIAA J. **12**, 826–831 (1974).
36. M. A. Woodmansee, R. P. Lucht, and J. C. Dutton, "Stark broadening and stimulated Raman pumping in high-resolution n coherent anti-Stokes Raman scattering spectra," AIAA J. **40**, 1078–1086 (2002).
37. D. A. Greenhalgh and S. T. Whittley, "Mode noise in broadband CARS spectroscopy," Appl. Opt. **24**, 907–913 (1985).
38. T. Seeger, M. C. Weikl, F. Beyrau, and A. Leipertz, "Identification of spatial averaging effects in vibrational CARS spectra," J. Raman Spectrosc. **37**, 641–646 (2006).
39. M. Playez and D. Fletcher, "Free stream test conditions determination in ICP wind tunnels using the TALIF measurement technique," in *40th AIAA Thermophysics Conference* (2008), paper AIAA 2008-4254.
40. F. Zander, T. Marynowski, and S. Loehle, "High-speed imaging of high-frequency effects of a $CO_2$ plasma flow," J. Thermophys. Heat Transfer **31**, 451–462 (2017).
41. D. R. Snelling, R. A. Sawchuk, and T. Parameswaran, "Noise in single-shot broadband coherent anti-Stokes Raman spectroscopy that employs a modeless dye laser," Appl. Opt. **33**, 8295–8301 (1994).
42. T. Seeger and A. Leipertz, "Experimental comparison of single-shot broadband vibrational and dual-broadband pure rotational coherent anti-Stokes Raman scattering in hot air," Appl. Opt. **35**, 2665–2671 (1996).
43. S. P. Kearney, K. Frederickson, and T. W. Grasser, "Dual-pump coherent anti-Stokes Raman scattering thermometry in a sooting turbulent pool fire," Proc. Combust. Inst. **32**, 871–878 (2009).
44. D. R. Richardson, R. P. Lucht, W. D. Kulatilaka, S. Roy, and J. R. Gord, "Theoretical modeling of single-laser-shot, chirped-probe-pulse femtosecond coherent anti-Stokes Raman scattering thermometry," Appl. Phys. B **104**, 699–714 (2011).
45. A. Bohlin and C. J. Kliewer, "Communication: two-dimensional gas-phase coherent anti-Stokes Raman spectroscopy (2D-CARS): simultaneous planar imaging and multiplex spectroscopy in a single laser shot," J. Chem. Phys. **138**, 221101 (2013).
46. S. P. Kearney, "Hybrid fs/ps rotational CARS temperature and oxygen measurements in the product gases of canonical flat flames," Combust. Flame **162**, 1748–1758 (2015).
47. R. D. Hancock, K. E. Bertagnolli, and R. P. Lucht, "Nitrogen and hydrogen CARS temperature measurements in a hydrogen/air flame using a near-adiabatic flat-flame burner," Combust. Flame **109**, 323–331 (1997).
48. F. Vestin and P.-E. Bengtsson, "Rotational CARS for simultaneous measurements of temperature and concentrations of $N_2$, $O_2$, CO, and $CO_2$ demonstrated in a co/air diffusion flame," Proc. Combust. Inst. **32**, 847–854 (2009).
49. B. R. Greene, "Simulation of pyrolysis gas in a charring ablative thermal protection material using gas injection through a porous graphite sample," Ph.D. thesis (The University of Texas at Austin, 2018).